Electroless tin and polymer layers synergize for lithium dendrite suppression and cycling lifespan enhancement

Junqian Bai[a,b], Yuanjun Wang[a,b], Hao Yu[a,b], ChaoHui Wei[b*], Weijia Zhong[a], Shuqin He[a], Qiang Zhao[a], Aijun Zhou[a,b], and Jingze Li[a,b*]

a School of Materials and Energy, University of Electronic Science and Technology of China, Chengdu 611731, P. R. China

b Huzhou Key Laboratory of Smart and Clean Energy, Yangtze Delta Region Institute (Huzhou), University of Electronic Science and Technology of China, Huzhou 313001, P. R. China

Corresponding author E-mail: lijingze@uestc.edu.cn (J. Z. Li)

Experimental section

Chemical reagents

The chemical stannous chloride ($SnCl_2 \cdot 2H_2O$, 98.0%) was purchased from Shanghai Aladdin Biochemical Technology Co., LTD. Trisodium citrate dihydrate ($C_6H_5Na_3O_7 \cdot 2H_2O$, 99.0%), sodium hypophosphite (NaH_2PO_2, 98.0%) and thiourea (CH_4N_2S, 99.0%) were purchased from Shanghai Maclin Biochemical Technology Co., LTD. Polyacrylic acid (PAA, 99.0%), dimethyl sulfoxide (DMSO, 99.9%) and Octylphenol ethoxylate (OP-10) were purchased from Shanghai Meryer Chemical Technology Co., LTD. Lithium (Li, 99.9%) was purchased from Chengdu Denway Newtype Metal Material Co., Ltd. Copper (Cu, 99.9%) was purchased from Shenzhen Wantong Meixin Technologies Co., Ltd.

Preparation method of electroless tin plating solution

1.805 g of $SnCl_2 \cdot 2H_2O$, 1.647 g of $C_6H_5Na_3O_7 \cdot 2H_2O$, 4.927 g of NaH_2PO_2, and 7.308 g of CH_4N_2S were sequentially added to 80 mL of deionized water. Subsequently, 3.0 mL of 37% HCl and 2.0 mL of OP-10 were supplemented into the above mixture. The resulting solution was stirred thoroughly at a constant temperature of 60 ℃ for 12 h to form a homogeneous electroless tin-plating bath.[1]

Preparation of electrodes

Firstly, wipe the surface of the Cu foil with anhydrous ethanol to remove organic substances. Then, immerse in dilute sulfuric acid for thorough cleaning to remove surface impurities and oxide layers. Following that, the cleaned Cu foil was immersed in the electroplating solution for 5 min in a constant-temperature bath maintained at 60 ℃. After that, place in a 60 ℃ vacuum oven for overnight drying. Finally, directly cut into a 12 mm diameter circular piece to obtain the Cu/Sn

electrode.

For the fabrication of the Cu/Sn/PAA electrode, apply 20 μL of the solution (a DMSO solution containing 0.1 wt% PAA) onto the surface of the Cu/Sn electrode and then dry under vacuum at 60 ℃ to obtain the Cu/Sn/PAA electrode.

Characterization of electrochemical performance

To evaluate the electrochemical performance of the prepared electrodes, CR2032 button cells were assembled in an argon atmosphere glove box. The electrolyte was prepared by dissolving 1 M LiTFSI (dibutyl trifluoromethanesulfonimide lithium) in a mixture of DME (1,2-dimethoxyethane) and DOL (1,3-dioxolane) (volume ratio 1:1), and 2 wt% $LiNO_3$ was added as an additive. The separator was Celgard 2325. All constant current charge-discharge tests were conducted under the Neware battery testing system. Among them, the half-cell was cycled at a fixed capacity of 1 mAh cm^{-2}, with current densities of 0.5, 1, and 2 mA cm^{-2}, respectively; the symmetric cell consisted of the desired electrodes with pre-deposited 4 mAh cm^{-2} metallic Li, and then was cycled at a fixed areal capacity of 1 mAh cm^{-2} at a current density of 1 mA cm^{-2}; the full-cell utilized a $LiFePO_4$ (LFP) positive electrode with a mass loading of 12.3 mg cm^{-2}, and was cycled in the voltage window of 2.5-3.8 V (vs. Li/Li^+) at 1 C. Additionally, all electrochemical tests were completed on the CHI660E electrochemical workstation (Shanghai Chenhua). Specifically, the tests included: electrochemical impedance spectroscopy (EIS) tests with a frequency range of 10^{-2} Hz to 10^5 Hz and an amplitude voltage of 10 mV; Tafel curve measurements with a scan rate of 0.5 mV s^{-1}; cyclic voltammetry (CV) tests with a scan rate of 0.1 mV s^{-1} and a potential window of 0-2.0 V (vs. Li/Li^+).

Material characterization

The sample morphology, microstructure and element distribution were characterized by a field emission scanning electron microscope (FE-SEM, Phenom pharos) equipped with an energy dispersive X-ray spectrometer (EDS). The electrodes after cycling were rinsed with DME solvent and dried under vacuum in a glove box for subsequent analysis. X-ray diffraction (XRD, MiniFlex600) was performed using a Cu Kα radiation source (λ = 0.154 nm) with a scanning rate of 10° min^{-1}, collecting data within the range of 2θ = 10°-90°. In-situ optical observation was accomplished using a 20x objective lens of a digital microscope (Zeiss Axioscope 5/Axiolab 5), and Raman spectroscopy was collected by a spectrometer (XploRA PLUS, HORIBA).

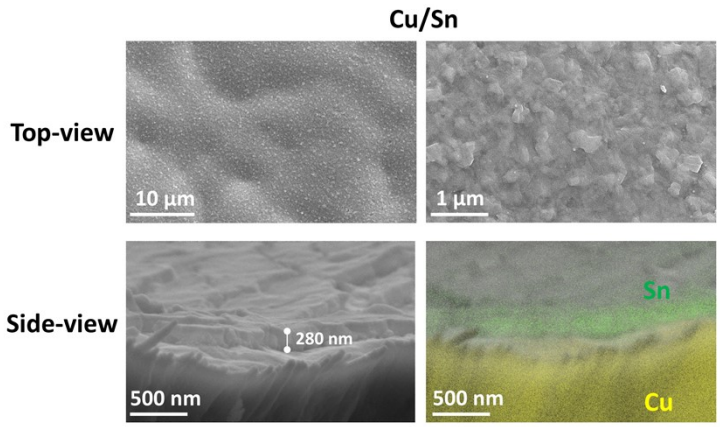

Fig. S1. Top-view and side-view SEM images of Cu/Sn electrode.

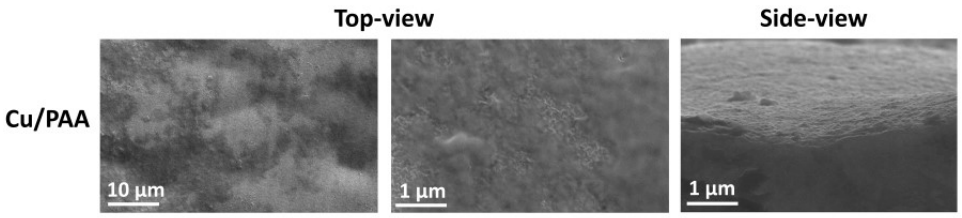

Fig. S2. Top-view and side-view SEM images of Cu/PAA electrode.

The key characteristic peak regions corresponding to the PAA characteristic peaks (~1690 cm^{-1} and ~1450 cm^{-1}) of the Cu/PAA and Cu/Sn/PAA electrode, can be observed in the Raman spectra (Fig. S3).[2] These findings suggest the successful affiliation of PAA polymer as an interface stabilizer on the electrode surface.

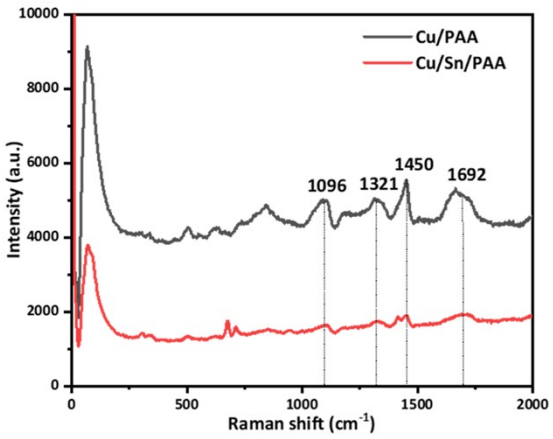

Fig. S3. Raman spectra of Cu/PAA and Cu/Sn/PAA electrodes.

Fourier transform infrared (FT-IR) spectra were further collected to verify the in-situ formation of ion-conductive LiPAA via the interfacial reaction between PAA and metallic Li during cycling (Fig. S4). The characteristic peak assigned to lithium carboxylate (-COOLi) is stably detected on the Cu/PAA-Li anode before and after cycles, directly confirming the formation and structural stability of LiPAA during cycling.[3]

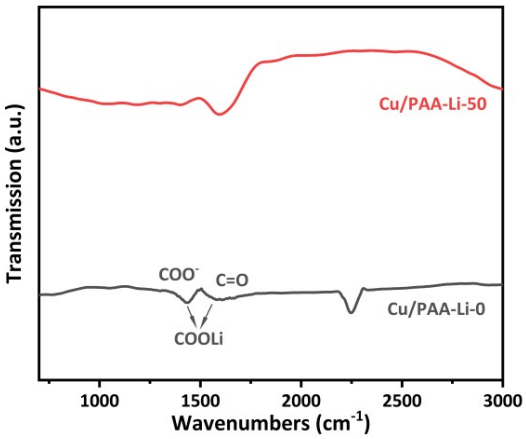

Fig. S4. Fourier transform infrared (FT-IR) spectra of the Cu/PAA-Li electrodes before and after cycling.

To evaluate the mechanical stability of the Cu/Sn/PAA composite electrode, a bending test was performed (Fig. S5).[4] The bare Cu foil showed irreversible deformation after bending and could not recover, while the Cu/Sn/PAA electrode exhibited excellent mechanical resilience and fully recovered to its original state. This good flexibility enables the electrode to better accommodate the volume change of Li metal anode during cycling.

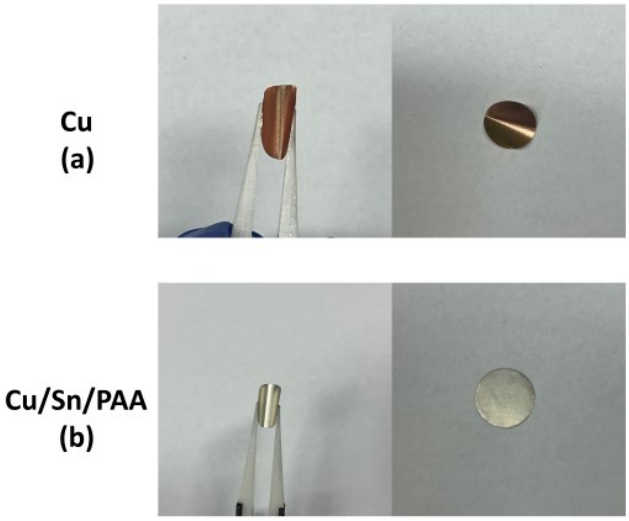

Fig. S5. Digital photographs of the mechanical flexibility test (a) Cu foil and (b) Cu/Sn/PAA electrode under bending.

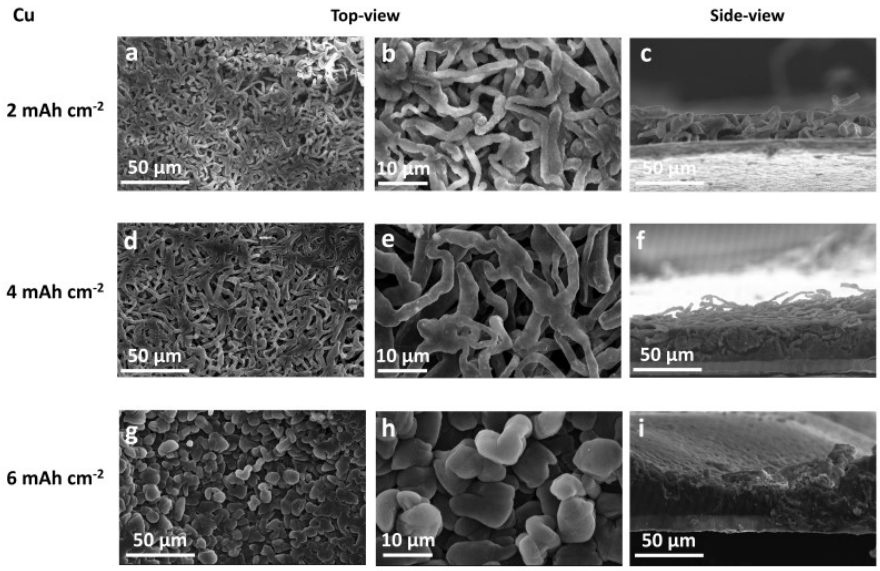

Fig. S6. Top-view and side-view SEM images of Li plated with (a-c) 2 mAh cm^{-2}, (d-f) 4 mAh cm^{-2} and (g-i) 6 mAh cm^{-2} on bare Cu electrodes at 0.5 mA cm^{-2}.

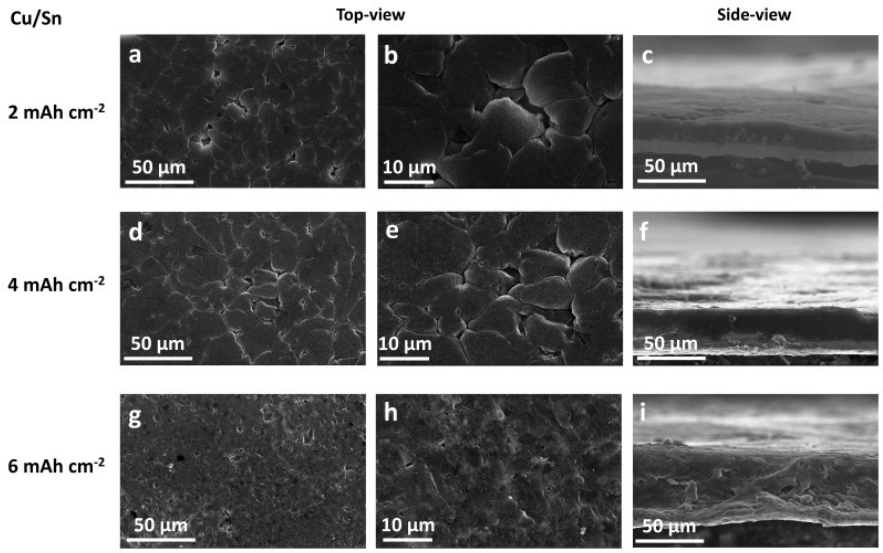

Fig. S7. Top-view and side-view SEM images of Li plated with (a-c) 2 mAh cm^{-2}, (d-f) 4 mAh cm^{-2} and (g-i) 6 mAh cm^{-2} on Cu/Sn electrodes at 0.5 mA cm^{-2}.

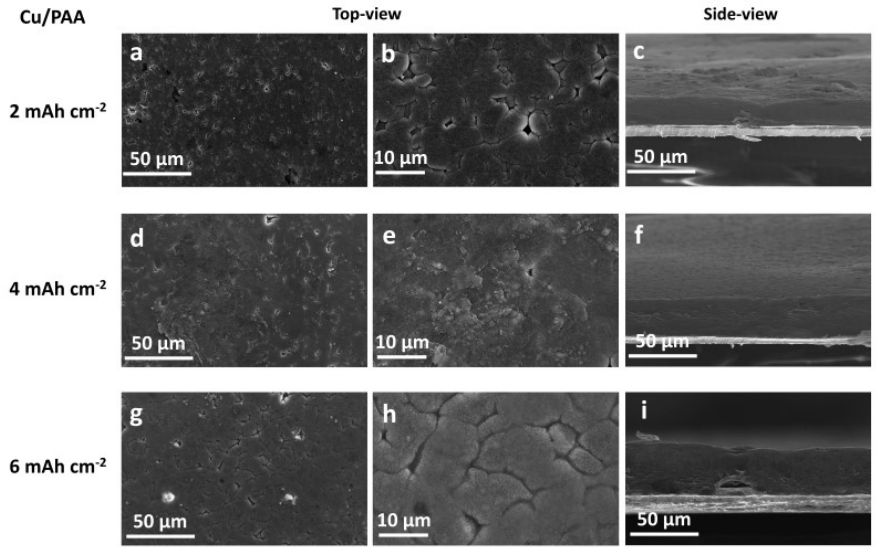

Fig. S8. Top-view and side-view SEM images of Li plated with (a-c) 2 mAh cm^{-2}, (d-f) 4 mAh cm^{-2} and (g-i) 6 mAh cm^{-2} on Cu/PAA electrodes at 0.5 mA cm^{-2}.

The electrolyte wettability difference on these electrodes was verified by contact angle tests (Fig. S9). The Cu/Sn/PAA electrode delivers a significantly reduced electrolyte contact angle of ~4.8° compared with bare Cu foil (~18°), demonstrating the greatly enhanced interfacial wettability, which is conducive to the uniform distribution of Li^+ flux at the electrode/electrolyte interface.

Fig. S9. Contact angles of electrolyte on the Cu, Cu/Sn, Cu/PAA and Cu/Sn/PAA surfaces.

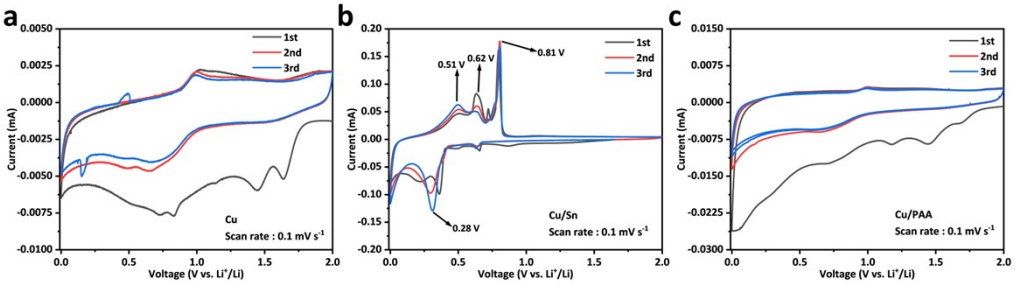

Fig. S10. CV curves of (a) Li|Cu, (b) Li|Cu/Sn and (c) Li |Cu/PAA half-cells at a scanning rate of 0.1 mV s^{-1}.

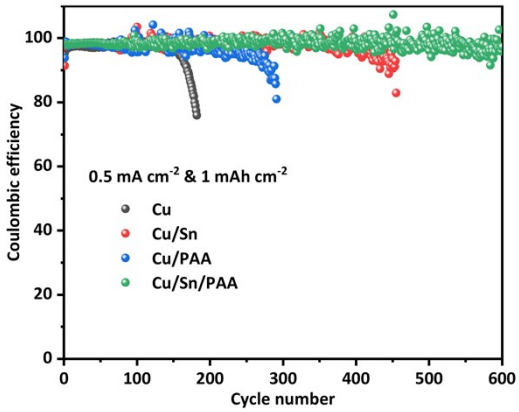

Fig. S11. CE of the Cu, Cu/Sn, Cu/PAA, and Cu/Sn/PAA electrodes at 0.5 mA cm^{-2} and 1 mAh cm^{-2}.

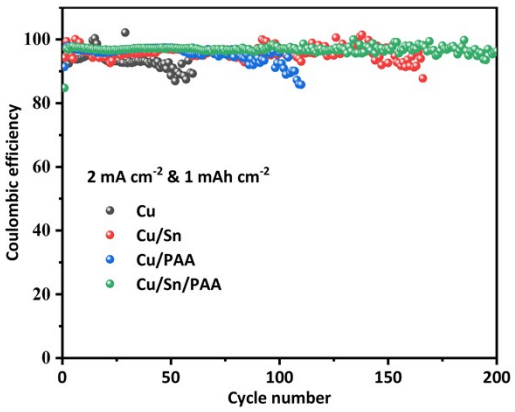

Fig. S12. CE of the Cu, Cu/Sn, Cu/PAA, and Cu/Sn/PAA electrodes at 2 mA cm^{-2} and 1 mAh cm^{-2}.

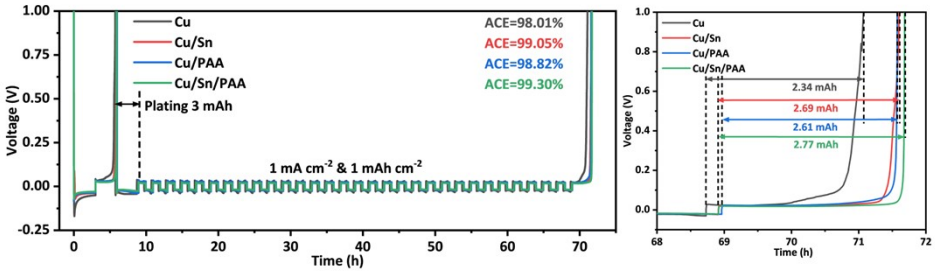

Fig. S13. (a) ACE test for 30 cycles of Li stripping/deposition at 1 mA cm^{-2} and 1 mAh cm^{-2}; (b) the final delithiation process after 30 cycles.

The Tafel polarization curves and electrochemical impedance spectroscopy (EIS) tests were conducted to analyse the intrinsic kinetic performances and interfacial resistance. Based on the Tafel curves, the exchange current density (j_0) directly reflects the kinetic rate of interface charge transfer, where a higher j_0 value suggests faster Li^+ migration, more uniform flux distribution and lower electrochemical polarization.[5] The j_0 (0.914 mA cm^{-2}) of the Cu/Sn/PAA-based electrode was significantly enhanced as compared to bare Cu-based electrode (0.447 mA cm^{-2}, Fig. S9). Furthermore, the interfacial impedance of Cu/Sn/PAA electrode from EIS tests was obviously lower than the bare Cu foil electrode both before cycling and after 50 cycles (Fig. S10), consistent with the Tafel analysis. The electrochemical stability of Cu/Sn/PAA-Li anode was systematically evaluated via the galvanostatic cycling (1 mA cm^{-2}, 1 mAh cm^{-2}) and rate performance tests in symmetric cells.

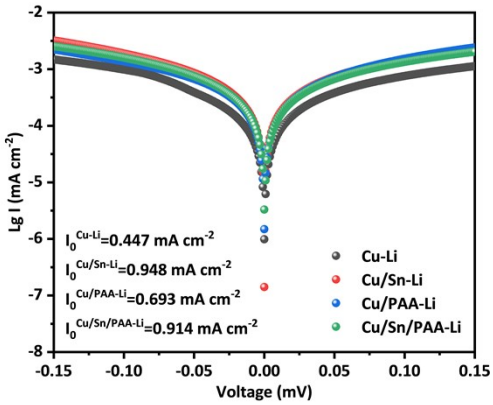

Fig. S14. Tafel curves of Cu-Li, Cu/Sn-Li, Cu/PAA-Li, and Cu/Sn/PAA-Li symmetrical cells.

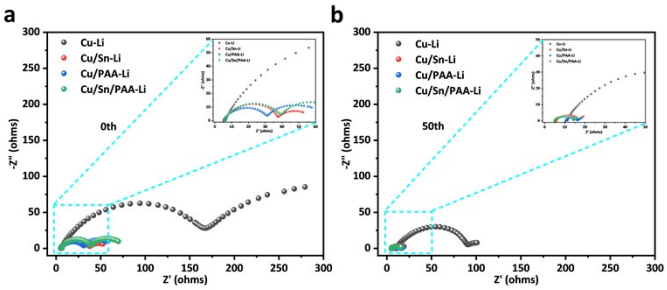

Fig. S15. (a) Nyquist plots of Cu-Li, Cu/Sn-Li, Cu/PAA-Li, and Cu/Sn/PAA-Li symmetrical cells before cycling and (b) after 50 cycles.

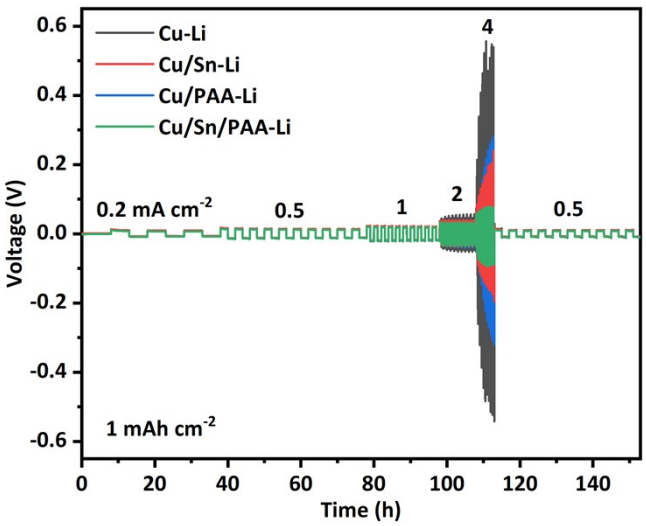

Fig. S16. Rate performance of Cu-Li, Cu/Sn-Li, Cu/PAA-Li, and Cu/Sn/PAA-Li symmetrical batteries at different current densities.

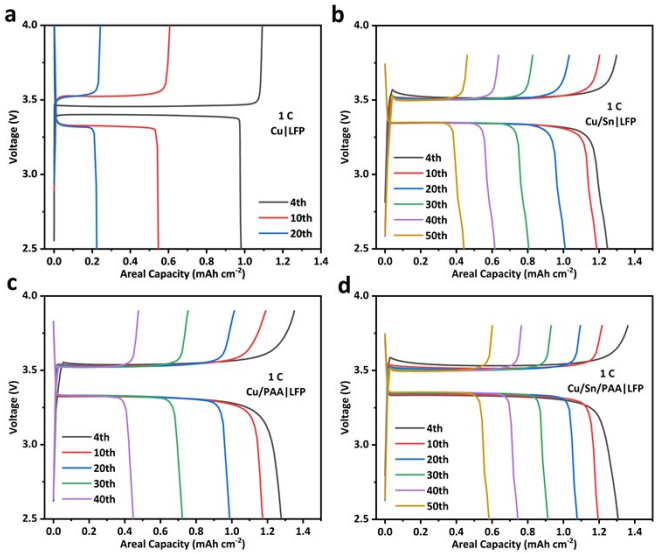

Fig. S17. The typical charge/discharge curves of Cu|LFP (a), Cu/Sn|LFP (b), Cu/PAA|LFP (c), Cu/Sn/PAA|LFP (d) at 1 C.

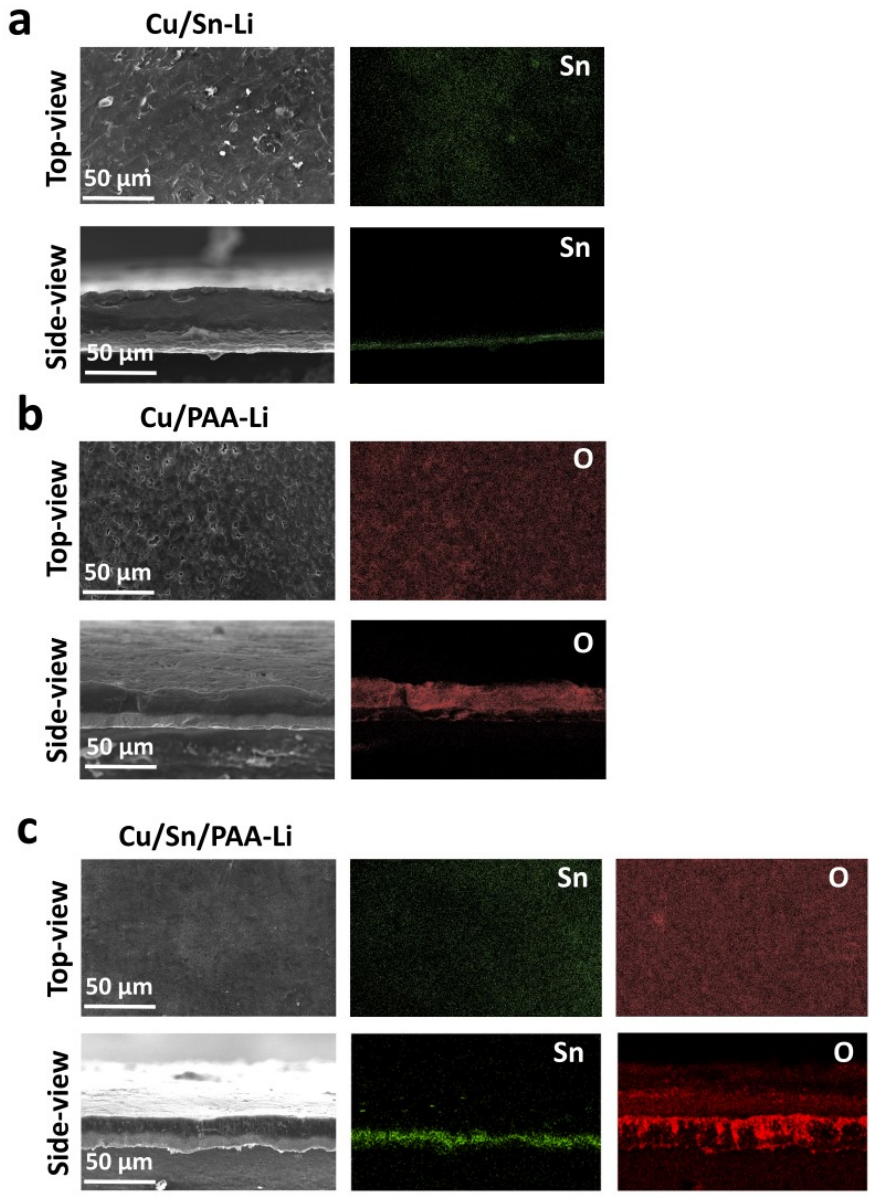

Fig. S18. Top-view and side-view SEM images and corresponding EDS elemental mapping of the electrodes after 50 Li plating/stripping cycles: (a) Cu/Sn-Li electrode (Sn elemental mapping), (b) Cu/PAA-Li electrode (O elemental mapping), (c) Cu/Sn/PAA-Li electrode (Sn and O elemental mapping).

X-ray photoelectron spectroscopy (XPS) characterization was further performed to analyze the compositions of the SEI layer on the four electrodes after 50 cycles. The high-resolution C 1s spectra of all samples can be deconvoluted into four characteristic peaks, corresponding to the C-C bond at 284.8 eV, C-OR bond at ~286.5 eV, COOR (lithium carboxylate) bond at ~288.2 eV, and CO_3^{2-} (lithium carbonate) species at ~290.0 eV.[3] By comparing the C 1s results, we found that the bare Cu-Li electrode after cycling shows a significantly higher proportion of oxygen-containing components (C-OR, COOR, CO_3^{2-}) in the SEI, indicating severe parasitic decomposition of the electrolyte during cycling and the formation of a large amount of unstable organic/inorganic SEI by-products. In contrast, for the Cu/Sn/PAA-Li electrode, the peak intensities of these oxygen-containing by-products are remarkably reduced. Meanwhile, a distinct characteristic peak of lithium carboxylate corresponding to in-situ formed LiPAA is observed, which clearly demonstrates the formation of LiPAA-derived SEI on the electrode surface after cycling, effectively suppressing the continuous decomposition of the electrolyte.

For the high-resolution F 1s spectra, the characteristic peak at ~685 eV is assigned to LiF derived from electrolyte decomposition, and the peak at ~688 eV corresponds to the C-F species.[6] The comparative results show that the intensity of the LiF peak increases gradually by the electrode modification (from Cu-Li to Cu/Sn-Li, Cu/PAA-Li, and finally Cu/Sn/PAA-Li), with the strongest LiF signal obtained on the Cu/Sn/PAA-Li electrode. On the contrary, the intensity of the C-F peak shows an opposite trend, with the lowest proportion of C-F species in the SEI of the Cu/Sn/PAA-Li electrode. It is widely accepted that LiF is a critical inorganic SEI component with high mechanical strength and excellent interfacial stability, while C-F species are mostly derived from incomplete decomposition of lithium salt and unstable residues in the SEI. The above F 1s results confirm that the Cu/Sn/PAA composite can induce the formation of more stable LiF during cycling and reduce the generation of unstable C-F by-products, thus constructing a SEI film with more stable composition and uniform structure.

In brief, the XPS results clearly reveal the significant difference in SEI composition among the four electrodes. The Cu/Sn/PAA-Li electrode develops a stable SEI upon cycling, characterized by LiPAA-derived organic components and a high-content of LiF as the inorganic component.Compared with the unmodified and single-component modified electrodes, the Cu/Sn/PAA-Li electrode effectively inhibits the parasitic side reactions of the electrolyte and

prohibits the formation of unstable SEI components. The stable SEI works synergistically with the lithiophilic Li-Sn alloy, endowing the electrode with outstanding interfacial stability, which is consistent with our electrochemical test results.

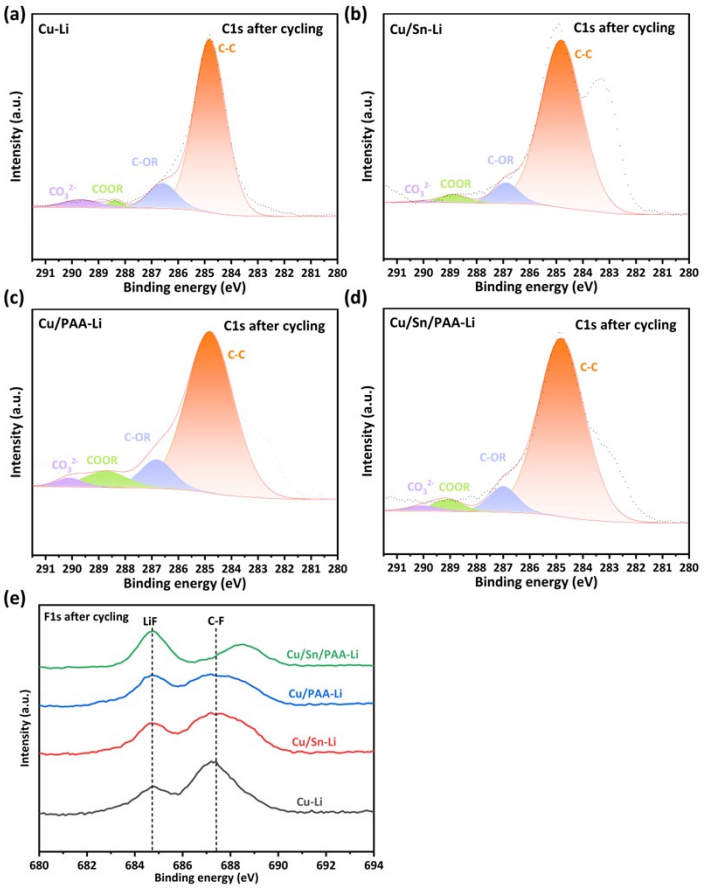

Fig. S19. XPS spectra of four different electrodes after 50 cycles of Li plating/stripping: (a-d) C1s curves with peak fitting of (a) Cu-Li, (b) Cu/Sn-Li, (c) Cu/PAA-Li and (d) Cu/Sn/PAA-Li electrodes; (e) F1s curves of the corresponding four electrodes.

Table S1. Electrochemical performance comparison between this work and recently reported work.

Electrode	Current ($mA\ cm^{-2}$)	Capacity ($mAh\ cm^{-2}$)	Average CE value	Cycle number	Reference
MgF_2/Au-coated Cu	1	1	98.85%	150	Energy Storage Materials, 2026, 85, 104883
Cu-HEA-F	0.5	1	96%	150	Energy Storage Materials, 2025, 81, 104497
PDA@Cu-30	1	1	97.8%	200	Journal of Energy Storage, 2025, 132, 117854
TTA-COF-ZnF_2@Cu	1	1	98.4%	250	Journal of Energy Chemistry, 2025, 105, 407-417
Cu@CuO-PAN	0.2	0.2	98%	100	Ceramics International, 2025, 51, 22879-22885
PVDF/LiF−Ag@Cu	1	1	98.2%	130	ACS Applied Energy Materials, 2023, 6, 519-529
Cu/Sn/PAA	**1**	**1**	**98.21%**	**400**	**This work**

Notes and reference

1. K. X. Liu, R. Tan, Z. Zheng, R. R. Zhao, B. Ülgüt, X. P. Ai and J. F. Qian, *Rare Metals*, 2025, **44**, 81-94.
2. B. Han, M. J. Piernas-Muñoz, F. Dogan, J. Kubal, S. E. Trask, I. D. Bloom, J. T. Vaughey and B. Key, *J. Electrochem. Soc.*, 2019, **166**, A2396.
3. N. W. Li, Y. Shi, Y. X. Yin, X. X. Zeng, J. Y. Li, C. J. Li, L. J. Wan, R. Wen and Y. G. Guo, *Angew. Chem. Int. Ed.*, 2018, **57**, 1505-1509.
4. N. T. Temesgen, W. A. Tegegne, K. N. Shitaw, F. W. Fenta, Y. Nikodimos, B. W. Taklu, S. K. Jiang, C. J. Huang, S. H. Wu, W. N. Su and B. J. Hwang, *Taiwan Inst. Chem. Eng.*, 2021, **128**, 87-97.
5. Z. Wang, T. Chen, Z. Song, J. Xing, A. Zhou and J. Li, *Energy Mater.*, 2024, **4**, 400031.
6. S. K. Merso, T. M. Tekaligne, M. Adigo Weret, K. N. Shitaw, Y. Nikodimos, S. C. Yang, Z. B. Muche, B. W. Taklu, B. T. Hotasi, C. Y. Chang, S. K. Jiang, G. Brunklaus, M. Winter, S. H. Wu, W. N. Su, C. Y. Mou and B. J. Hwang, *Chem. Eng. J.*, 2024, **485**, 149547.